Polyelectrolyte Spin Assembly: Influence of Ionic Strength on the Growth of Multilayered Thin Films

CHRISTOPHE J. LEFAUX,[1] JESSICA A. ZIMBERLIN,[2] ANDREY V. DOBRYNIN,[1,3] PATRICK T. MATHER[1,2]

[1]Polymer Program, Institute of Materials Science, University of Connecticut, Storrs, Connecticut 06269

[2]Chemical Engineering Department, University of Connecticut, Storrs, Connecticut 06269

[3]Physics Department, University of Connecticut, Storrs, Connecticut 06269

Received 7 January 2004; revised 12 March 2004; accepted 20 March 2004
DOI: 10.1002/polb.20209
Published online in Wiley InterScience (www.interscience.wiley.com).

ABSTRACT: Layer-by-layer (LbL) assembly of polymer electrolyte multilayers is now a well-established method for the fabrication of thin films by sequential adsorption of alternating layers of oppositely charged polyelectrolytes. Most commonly, such adsorptions have been from quiescent solutions of varying ionic strength and pH. Here, we report results on an alternative processing route for the achievement of polymeric multilayer assemblies of poly(sodium-4-styrene sulfonate) and poly(allylamine hydrochloride) that utilizes conventional spin coating. We investigated and describe herein the dependence of multilayer film buildup on solution ionic strength for comparison with similar dependence in quiescent adsorption. Using UV-Vis spectroscopy we monitored the growth of the multilayered films, while with Atomic Force Microscopy (AFM) we examined the surface features and measured coating thicknesses at different salt concentrations. AFM and UV-Vis data reveal two regimes of behavior with increasing salt: strong salt-dependence at low salt contents, and weak salt-dependence for high salt contents. To explain this observation, we introduce the relevance of the dimensionless group $De = \dot{\gamma}\tau$, the local Deborah Number, to the problem. As ionic strength increases, τ increases so that spin-assembly flow influences adsorbed conformation, and thus LbL growth rate. Our results indicate the ability to design and control polyelectrolyte multilayered structures prepared via spin assembly by varying solution properties that influence the conformation of deposited polymer chains. Additionally, our studies reveal the need for study of the fundamental mechanisms of polyelectrolyte adsorption within complex flow fields. © 2004 Wiley Periodicals, Inc. J Polym Sci Part B: Polym Phys 42: 3654–3666, 2004

Keywords: layer-by-layer assembly; polyelectrolytes; multilayers; spin coating

INTRODUCTION

The layer-by-layer (LbL) deposition of charged objects was first reported in 1966[1] for colloidal particle assembly and later rediscovered in the early 1990s for polyelectrolytes.[2,3] This directed assembly technique is based on the long-range electrostatic attraction between oppositely charged molecules, and has been introduced for fabrication of the molecularly layered multicomponent thin films with seemingly unlimited complexity. The interested reader is referred to several review articles on this subject.[4–7] The key to a successful deposition of multilayer assemblies in a layer-by-layer fashion is the achievement of

Correspondence to: P.T. Mather (E-mail: Patrick.mather@uconn.edu)

Journal of Polymer Science: Part B: Polymer Physics, Vol. 42, 3654–3666 (2004)

charge inversion and subsequent reconstruction of surface properties at each step of the process. For example, this can be achieved by first immersing ("dipping") a substrate into a dilute aqueous solution of cationic (or anionic) polyelectrolytes for a period of time required for adsorption of the layer of given thickness, followed by rinsing in water. The rinsing step is necessary to remove the polymers that are not tightly adsorbed to the substrate. During the next step, the same substrate that is now covered with adsorbed polyelectrolytes is exposed to a dilute solution of complementary anionic (or cationic) macromolecules, and again rinsed. The result is a more or less irreversibly adsorbed bilayer whose interpenetration and thickness are sensitive to polyelectrolyte charge, ionic strength, and adsorption time. LbL processing ensues by repetition of this process many times to thus build up multilayers with thicknesses spanning 100 to 1000 Å, or 10 to 30 Å per bilayer step. Interestingly, the observed buildup is found to depend on solution conditions, such as pH or ionic strength. For example, it has been reported that multilayered films produced with high salt concentration are thicker, and have a higher surface roughness than without salt when obtained using the dipping LbL method.[8,9]

Although a robust and well-tested processing route, it is generally recognized that the dipping LbL approach to multilayer deposition is excessively time-consuming—each complete process requiring hours to complete and robotic equipment for acceptable reproducibility. Additionally, it has been found that the dipping method yields a relatively high roughness, compared to methods introduced below, in the resulting multilayered thin coating.[5,10] Considering this throughput limitation, some effort has been directed toward developing more rapid processing schemes that still exploit electrostatic adsorption. An obvious selection has been the spin-coating method, a process that offers an alternative approach to a dipping deposition of alternating layers. Here, a spin coater is operated in a conventional manner with excess solution (polycation or polyanion) applied to a substrate before spinning, during which time solution is first rapidly (<1 s) expelled from the surface, following which a thin film of polyelectrolyte solution more slowly thins and dries over the course of 2–10 s. To build up polyelectrolyte multilayers in an LbL fashion, this spin-coating step is applied sequentially to solutions of oppositely charged polyelectrolytes with intervening rinsing steps also achieved using the spin coater. It was shown recently[11–13] that such a method, here termed polyelectrolyte spin assembly (PSA), allows for rapid processing and for uniform coating of the substrate. Furthermore, the process is found to produce highly ordered coatings that are smoother and thicker when compared with the coatings attained by dipping technique applied to identical solutions.[3,11]

How might spin coating afford more rapid processing? Although equilibrium adsorption is achieved after 10–20 min in quiescent adsorption that transpires by diffusion from solution, PSA leads to apparent complete adsorption with charge inversion after only one step (2–10 s) as promoted by convection and hydrodynamic stress. The centrifugal force induced by the fast spinning rate and short spinning time, simultaneously drives out unassociated water and loosely bound polymer chains from the substrate. The combination of hydrodynamic shear stress due to flow, acting to distort adsorbing polymer chains, and electrostatic attraction between the polyelectrolytes and the oppositely charged substrate is thought to cause irreversible adsorption of highly ordered layers as evidenced by a high degree of surface planarization.[3,11] The combination of these effects produces a "thick" and highly dense layer of the charged polymers when compared to the dipping method. Direct comparisons of the two techniques by Hong's group has shown that the spin-assembly process yields faster buildup with substantial increase in polyelectrolyte adsorbed amount,[11] although a quantitative explanation was not provided.

The promise offered by PSA of rapid coating assembly has triggered research efforts directed toward elucidation of the effect of spin rate and polyelectrolyte concentration on multilayer deposition. In particular, Lee et al. have used UV-Vis spectroscopy and ellipsometry to reveal that layer thickness increases in proportion to polyelectrolyte concentration in a manner similar to quiescent (dipping) LbL processing. However, the proportionality constant—or slope of thickness versus cycle number—was larger for PSA than for the dipping deposition process.[13] The effect of spinning rate on the layer thickness increment for PSA of salt-free solutions was studied by Chiarelli et al.,[12] who found using ellipsometry that increasing the spin speed leads to thinner, perhaps more compacted, multilayers with an asymptotic behavior at high spin speeds. The observation was explained by the "increased mechanical forces" experienced by the films at higher spin-

ning rates that lead to a shorter contact time between polyelectrolyte solution and the substrate.

On the basis of the prior work summarized above, we hypothesized that the addition of salt to polyelectrolyte solutions processed by a spin assembly may lead to interesting results, as increasing salt addition for dipping LbL compared with increasing spin speed for a salt-free spin assembly have yielded opposite trends in growth rate. Thus, in this article, we report on the role of added salt in the polyelectrolyte spin-assembly process, especially regarding growth rate and ultimate surface morphology, using UV-Vis spectroscopy and AFM, respectively, and with consideration of the influence of added salt on chain structure preceding and during adsorption. A scaling theory is developed and found to be in good agreement with our experimental observations.

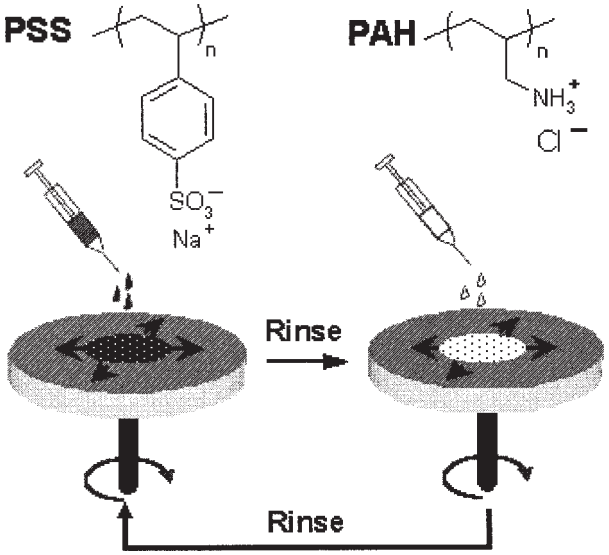

Scheme 1. Spin self-assembly process (3000 rpm during 8 s with a rinse step in between) and the chemical structures of the polyanion and polycation, poly(styrene sodium sulfonate) (PSS) and poly(allylamine hydrochloride) (PAH), respectively.

EXPERIMENTAL

Materials

The deposition of polyelectrolytes by spin assembly was performed on both quartz and silicon (100) substrates. Quartz substrates were 25.4 mm in diameter, while Si wafers were roughly square in shape with edge dimension of 10 mm. In both cases, substrates were treated with piranha solution (70:30 H_2SO_4/H_2O_2) at 80 °C for 1 h, followed by rinsing and sonication in ultrapure water for 15 min. After that cleaning step, surfaces were treated by a base treatment (1:1:5 $NH_3/H_2O_2/H_2O$) at 50 °C for 1 h, followed by a rinsing step in ultrapure water (Milli-Q, $\rho > 18$ MΩ · cm) for 15 min. To achieve the adsorption of the first polyelectrolyte layer and to produce a positively charged surface, a layer of low molecular weight poly(ethyleneimine) (PEI) was deposited on the substrate by spin coating at 3000 rpm for a duration of 8 s. The polyanion used in our experiments was poly(sodium 4-styrene sulfonate) (PSS), M_w = 70 kDa, and whose pKa is approximately 7. The polycation was poly(allylamine hydrochloride) (PAH), M_w = 15 kDa and pKa ~8.5. The structures of these polymers are shown in Scheme 1. The solution conditions, including pH ionic strength, were varied, and are detailed in the context of the experiments described.

Preparation of Multilayer Assemblies

The polyelectrolyte spin-assembly (PSA) process for a single cycle or "bilayer"—to be repeated multiple times—includes: (1) deposition of several drops of PSS solution to wet the whole charged surface followed by substrate spinning at 3000 rpm for 8 s (Scheme 1); (2) two washing steps with several drops each of pure deionized water at 3000 rpm for 8 s; (3) repetition of step (1) for PAH polyelectrolyte solution. The polymer deposition was performed using aqueous solutions with polymer concentration 10^{-2} *M*, on the basis of repeat unit molar mass, and pH = 3.5 adjusted with 0.1 *M* solution of HCl. At this pH, both the PSS and PAH are fully ionized.[14,15] The effect of salt concentration on the layer absorbance and thickness was studied for the following concentrations of NaCl: 0, 0.01, 0.05, 0.1, 0.5, and 2 *M*.

Characterization Techniques

UV-Vis Spectroscopy

UV-Vis spectra were collected with a Perkin-Elmer Lambda 6 spectrometer with a scan rate of 120 nm/min. A clean quartz disk with the same thickness as the spin-assembly substrate was used as a reference. The choice of PSS was dictated by its chromophoric nature that allows monitoring of the deposition process by UV-vis spectroscopy.[16] Thus, the amount of PSS in the spin-assembled films was monitored by UV-Vis

spectroscopy through the detection of the benzene $\pi \rightarrow \pi^*$ transition peak around 225 nm, with UV-Vis spectra being taken every two or five cycles of deposition, one cycle consisting of the consecutive deposition of PSS and PAH with a washing step in between (same speed). In contrast to PSS, PAH polymer shows no detectable feature in the UV-Vis spectrum. In most cases, we report the absorbance at the precise center of rotation for the disks; however, a radial dependence of multilayer thickness, and thus UV absorbance, was investigated by translation of the circular disk with respect to the beam along a line that intersected the disk center. For such measurements, it is pertinent that the beam diameter was approximately 1 mm.

Atomic Force Microscopy

The morphology, thickness, and surface roughness of the multilayer buildups were obtained using a Topometrix TMX 2000 Scanning Probe Microscope. The images were collected in the contact mode using model 1520-00 tips. Measurements were performed in air on dried film. Several images were recorded from different areas and representative images are being reported. The polymer film thickness was measured by scratching the multilayer assembly with a fresh razor blade and then scanning it with AFM to reveal a clear step at the scratch that is penetrates to the quartz substrate but no further.

Scaling Model

In the Appendix section, we derive expressions for the polymer surface coverage, Γ, and thickness, H, for each "bilayer" using a Flory-type theory. The starting point for the derivation is a free energy expression for adsorbing chains that includes, in the quiescent case, electrostatic, elastic, and binding terms. For steady growth, where each LbL cycle contributes equally to the surface coverage and thickness, minimization of this free energy predicts that the coverage per cycle follows:

$$\Gamma \approx m\sigma^* \approx \frac{\epsilon_a}{l_B r_D} \tag{1}$$

where ϵ_a s a dimensionless binding energy for ionic pair formation, l_B is the Bjerrum length, and r_D ($\sim c^{-1/2}$) is the Debye screening length. In our derivation, we have assumed that the interpenetration between two neighboring layers occurs at the length scale comparable with the Debye screening length. Such intermixing between the layers is driven by the electrostatic interactions that exists between oppositely charged chains and that is exponentially screened for distances larger than the Debye screening length. Further intermixing between layers is precluded by the formation of ionic pairs that significantly retard chain dynamics and the short duration of each deposition cycle.

In the presence of shear flow, the brush of adsorbed chains stretches and tilts from the normal direction. Additional chain extension occurs due to hydrodynamic drag on each chain section that forms a brush-like layer. Determination of the equilibrium conformation of a section of a chain under external shear flow requires balancing the hydrodynamic drag and electrostatic repulsion between charged monomers by the tension within such a section. However, the external flow is largely screened within each brush layer, the velocity field penetrating only a thin outer boundary layer whose thickness is comparable to the size of the outermost blob. The size of this blob is determined from the condition that the blob Deborah number $De_c = \dot{\gamma}\tau_e \approx 1$, where τ_e is the Zimm relaxation time of the last blob.[27,28] Thus, the extension of an adsorbed brush due to shear flow is localized to an outer region whose thickness is the size of the last blob. With these concepts (detailed in the Appendix), we arrive at the prediction,

$$\Gamma \approx \frac{\epsilon_a (r_D / l_B)}{r_D^2 + b^2(\dot{\gamma}\tau_o)^{2/3}} \tag{2}$$

where b is the Kuhn segment size, $\dot{\gamma}$ is the shear rate, and τ_o is a "bare" relaxation time for each Kuhn segment—generally an unknown quantity. The thickness per bilayer is predicted to follow a similar form. To fit experimental data, we may use the expression,

$$\Gamma \approx \alpha \frac{c^{-1/2}}{c^{-1} + \beta\dot{\gamma}^{2/3}} \tag{3}$$

where α and β should be considered to be fitting parameters, and c is the concentration of free ions in solution, including both added salt and polyelectrolyte counterions. Inspection of eq 3 reveals that in the no-flow limit $\Gamma \propto c^{1/2}$, while in the

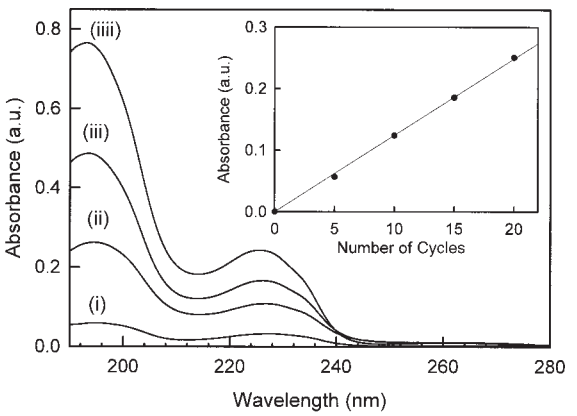

Figure 1. Plot of the absorbance versus wavelength of PSS/PAH (10^{-2} *M*, pH = 3.5) for a salt concentration of 0.1 *M* preparing by spin assembly at different number of bilayers: (i) 5 (i); (ii) 10; (iii) 15; and (iv) 20. Spin conditions: 3000 rpm, 8 s. Inset is peak absorbance (225 nm) versus cycle number of PSS/PAH (10^{-2} *M*, pH = 3.5) for 0.1 *M* NaCl concentration in both solutions. The solid line is a linear regression of the data.

strong-flow limit $\Gamma \propto c^{-1/2}$ with an intervening maximum.

Recognizing that in spin coating the shear rate close to the surface has a radial dependence:

$$\dot{\gamma} = \rho\omega^2 rh/\eta \tag{4}$$

where ρ is the solution mass density, ω is the angular velocity, r is the radial position, h is the instantaneous solution thickness, and η is the viscosity, eq 3 takes on a form that reveals both the spin speed and radial dependences:

$$\Gamma \approx \frac{\Gamma_o}{1 + \zeta(\omega^2 r)^{2/3}} \tag{5}$$

where Γ_o and ζ are fitting parameters. Below, we will make use of both eqs 3 and 5 in examination of the experimental data and to assess the level of consistency between our experiment and the simple theory.

RESULTS AND DISCUSSION

To elucidate the effect of salt concentration on the multilayer build up by the spin-assembly technique we have conducted a set of experiments at different ionic strengths. Figure 1 shows the dependence of absorbance on the number of deposition cycles for PSS/PAH system at pH = 3.5 and salt concentration 0.1 *M*. The amplitude of the absorbance peak at 225 nm shows a linear increase with the number of deposition cycles, indicating regular (linear) growth during spin-coating process (Fig. 1). We note that the lower wavelength absorption peak near λ = 195 nm has been reported before for a similar system,[17] and identified by one group to be an additional absorption from PSS.[18] Nevertheless, the linear relation between absorbance (at 225 nm) and polymer adsorbed amount allows us to evaluate how much polyelectrolyte was adsorbed on the substrate during each deposition cycle. Figure 2 shows growth curves for PSS/PAH spin-assembly for a range of salt concentrations. In all cases we have observed a linear increase in polymer's adsorbed amount with number of deposition cycles; however, the growth rates (slopes of the lines of Fig. 2) show saturation behavior described in more detail below.

The data shown in Figure 2 were obtained using UV-Vis transmission spectra where the transmitted beam was passed through the disk center. However, we have found a significant radial dependence of the absorbance, and thus coating mass. This dependence, shown in Figure 3, features a monotonically decreasing absorbance that follows an analytical form given in eq 5 (*vide supra*) using the absorbance at 225 nm for the surface coverage, Γ, and where r is the radial position in mm. The best fit to the data is obtained for parameters $\Gamma_0 = 0.298$ and $\zeta = 1.0 \cdot 10^{-4}$, but these parameters are sensitive to the poly-

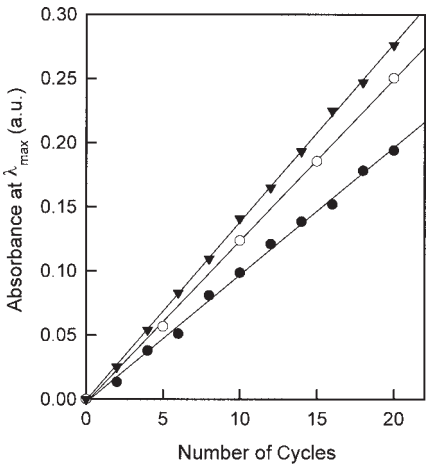

Figure 2. Plot of the absorbance at 225 nm versus the number of deposition cycles of PSS/PAH (C = 10^{-2} *M*, pH = 3.5) for varying NaCl concentration: No salt (●); 0.1 *M* (○); 2.0 *M* (▼) in both polyelectrolyte solutions preparing by spin assembly (3000 rpm, 8 s). Solid lines represent linear regressions.

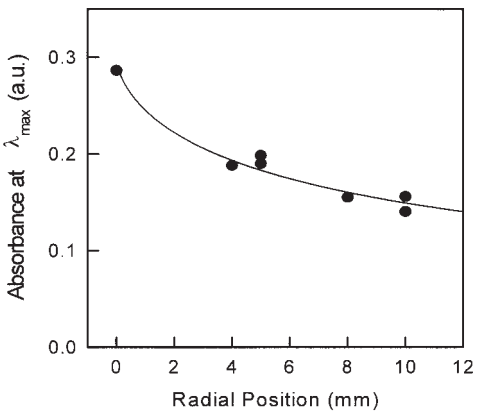

Figure 3. Radial dependence of the absorbance at 225 nm after 20 cycles of deposition of PSS/PAH ($C = 10^{-2}$ *M*, pH = 3.5) and NaCl concentration of 0.5 *M*. The solid line represents the best fit of eq 5 to the experimental data.

mer composition (absorbance) and solution details. It is noted that the multiple observations for positions 5 and 10 mm in Figure 3 were made at different azimuthal positions on the same disk. The basis of eq 5 is in the crossover from electrostatic to hydrodynamic dominance with increasing radius and is derived in the appendix. Although conventional spin coating of uncharged polymers leads to highly planarized coatings,[19,20] Chirelli et al.[12] found a similar radial dependence for spin-assembled polyelectrolytes, although a different functional form was selected to fit their data. Thus, it appears that such a radial gradient is unique to the PSA process, and should be an important clue in understanding the underlying mechanisms of coating growth. For simplicity, however, the rest of our study focuses on coatings examined at the axis of rotation, but with an aperture large enough (1 mm) to reveal flow effects.

Figure 4 show the dependence of PSA growth on salt as examined via absorbance from PSS at difference stages of multilayer growth. For low salt concentrations, the rate of LbL growth increases with increasing salt concentration, but then saturates (or reaches a broad maximum) for salt concentrations beyond 0.5 *M*. For higher salt concentrations, the growth rate becomes nearly constant, suggesting a dominant effect of hydrodynamic drag on the chain conformations. To show that the observed saturation behavior is independent of the number of deposition cycles, we plot in Figure 4 the absorbance at 10 and 20 cycles versus the salt concentration. Both sets of data reveal saturation beginning for concentrations greater than 0.5 *M*. We did not expect to observe such a plateau as shown in Figure 4. Indeed, eq 3 suggests that this plateau really represents a transition from electrostatic-dominated to hydrodynamic-dominated regimes, although for the parameters chosen we were unable to observe a regime for which $\Gamma \propto c^{-1/2}$. Higher rotation speeds should allow such observations.

The observed trends shown in Figure 4 are distinct from similar results reported in the literature for quiescent LbL processing. For the latter, is has been conjectured that ionic strength has a strong effect on the layering process through its effect on the structure of the polyelectrolytes in solution, with layers deposited at higher ionic strength being thicker, less interpenetrating, and less stable.[21] Dubas and Schlenoff have found an almost linear dependence of layer thickness on salt concentration[22] while Lvov and Decher reported that the layer thickness scales as the square root of ionic strength.[23] In the case of polyelectrolyte spin assembly, as discussed previously, the addition of shear forces caused by radial flow and a no-slip boundary condition should have a significant effect on chain conformation before and after adsorption and thus may explain the observed unique behavior.

To gain an understanding of the surface morphology, roughness, and thickness of the multilayered coatings, contact-mode AFM was conducted. To show typical results, we have selected AFM images of multilayered coatings obtained after 20 cycles of spin-coating PSS/PAH solutions on quartz substrates and with varying added

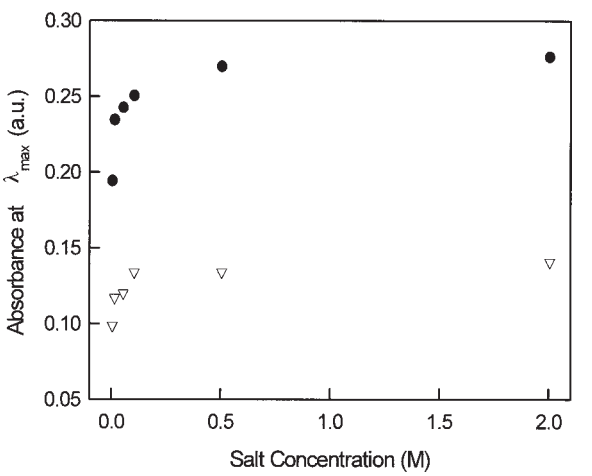

Figure 4. Absorbance values at 225 nm for 10 (▽) and 20 (●) spin assembly cycles of PSS/PAH (10^{-2} *M*, pH = 3.5) versus NaCl concentration. The reported absorbance was measured at the rotation axis center.

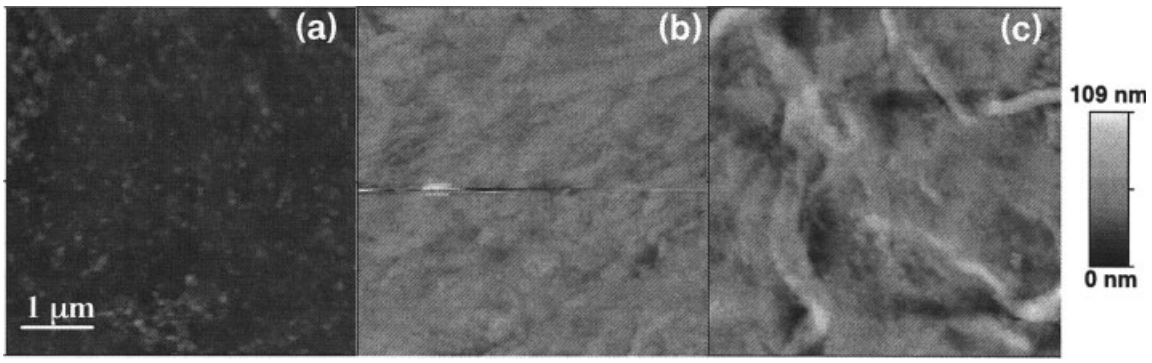

Figure 5. AFM images of the morphology of 20 bilayer films of PSS/PAH (10^{-2} *M*, pH = 3.5) deposited by the spin assembly process from: (a) 0 *M*, (b) 0.5 *M*, and (c) 2 *M* NaCl solutions.

NaCl concentration. The results are shown in Figure 5 where we observe that the coatings prepared using low salt concentration solutions are comparatively smooth, with only a slight granular texture as illustrated in Figure 5(a). Qualitatively, the surface roughness increases as salt concentration increases to 0.5 *M*, as shown in Figure 5(b), leading to significant roughness for the highest salt concentration of 2.0 *M*, with large features shown in Figure 5(c).

To quantify the AFM observations, we have employed height histogram analysis. Figure 6 shows histograms for the same AFM scans depicted in Figure 5; thus, for three different added salt concentrations of 0, 0.5, and 2 *M*. One can quickly see from the width of the distributions that the roughness of the coatings increases with ionic strength. In salt-free solutions the roughness (narrow width of the Gaussian peak) remained very low and indistinguishable from the underlying silicon substrate. But as salt concentration is increased, the height distribution becomes increasingly broadened, indicating rougher coatings. We quantified these observations by computing the root-mean-square roughness:

$$R_a = \sqrt{\frac{1}{N}\sum\left(h_i - \bar{h}\right)^2} \tag{6}$$

where N is the total number of height measurements, h_i is each height value, and $\bar{h}$ is the mean height. These data are plotted as inset to Figure 6 revealing a nearly linear increase in roughness with salt concentration. This is in contrast to the surface coverage measurements (Fig. 4), which showed clear saturation behavior with increasing salt. Presently, we have no theoretical model for roughness, but this key distinction should be captured in such a prediction.

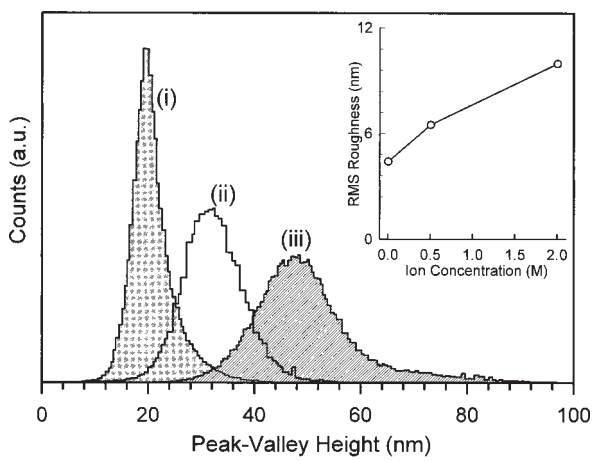

Figure 6. Peak-valley height distributions for different NaCl concentrations: (i) 0 *M*; (ii) 0.5 *M*; and (iii) 2 *M*. Inset is RMS roughness versus salt concentration.

Direct thickness measurements for the multilayered structures were obtained by scratching the surface with a fresh razor blade and then scanning the surface with contact mode AFM in a direction orthogonal to the scratch. An example result from this procedure is shown in Figure 7, with the darker region in the image being the substrate (where the film was removed by the razor plowing) and the bright regions are the multilayer stacks. The thickness of the film is obtained from the height difference between the substrate side and the multilayer stacks. Figure 8 shows the dependence of the layer thickness on the number of deposition cycles at different salt concentrations. There is a linear relationship between the layer thickness and the num-

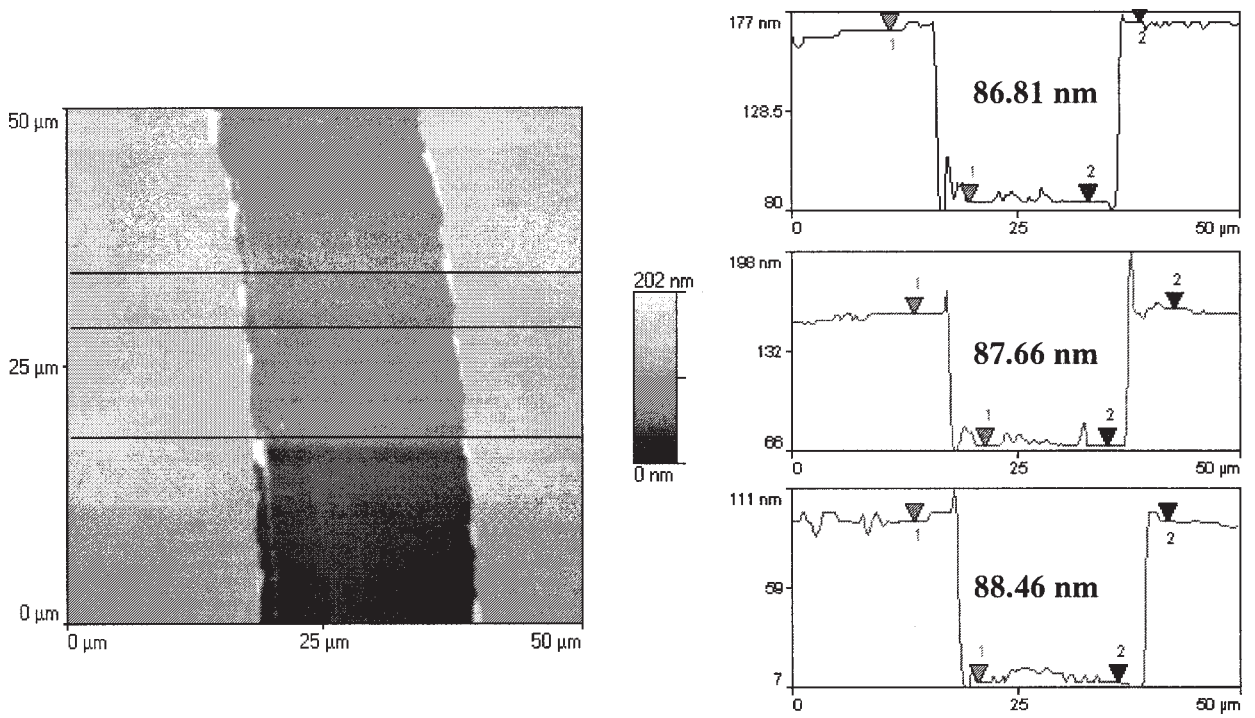

Figure 7. Thickness measurements are obtained by scratching with a razor blade to remove all the polyelectrolytes multilayer film. Dark side in the AFM image represents the scratch. Thickness measurements are made at several points (15 points). For instance, AFM from a 20 bilayers film of PSS/PAH (C = 10^{-2} *M*, pH = 3.5) with a 0.05 *M* salt concentration: Thickness 0.8831 ± 1.98 nm.

ber of deposition cycles for each salt concentration, as was observed for the surface coverage using UV absorption. For deposition from salt free solution, the slope is approximately 1.65 nm/bilayer, but the slope increases drastically with the addition of salt to be 4.73 nm/bilayer for 0.1 *M* salt, and saturates near 5.43 nm/ bilayer for 2 *M* solutions in a manner similar to the surface coverage measured with UV absorbance.

Both trends are clearly shown in Figure 9, where we plot the thickness and the absorbance growth rates versus the salt concentration. The dependence of thickness on salt concentration shows the same saturation behavior as one observed for UV-Vis measurement: the growth rate first increases as salt concentration increases then saturates beyond salt concentrations of approximately 0.5 *M*. For higher salt concentration the growth rate is independent of salt, indicating the dominant effect of hydrodynamic drag on the chain conformations.

CONCLUSIONS

In this study, we have examined a process termed polyelectrolyte spin assembly (PSA) by sequential spin coating of polyelectrolyte solutions using UV spectrometry and atomic force microscopy to study the growth, morphology, and roughness of the resulting coatings at different salt concentrations. Additionally a scaling theory was developed

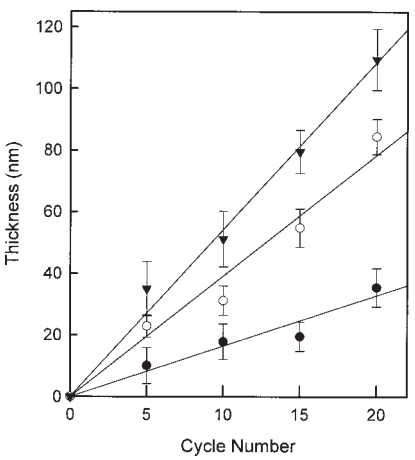

Figure 8. Thickness from AFM versus cycle number for spin assembly of PSS/PAH films using different salt concentrations: No salt (●); 0.01 *M* (○); and 2.0 *M* (▼). The solid lines represent linear regressions.

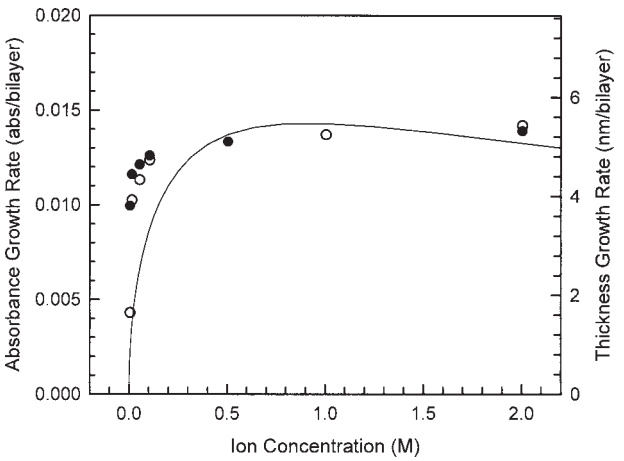

Figure 9. Thickness (○) and absorbance at 225 nm (●) at $(PSS/PAH)_{20}$ versus salt concentration, films prepared with Polyelectrolyte Spin Assembly method (3000 rpm, 8 s, C $=10^{-2}$ *M*, pH = 3.5).

that considers the compaction of adsorbing chains possible at the high shear rates involved in spin coating. Experimentally, PSA allowed rapid formation of polymeric multilayer structures to reveal trends in growth rate, which grew to saturation with increasing salt concentration and additionally showed drastic morphological alteration with salt addition. Additionally, a peculiar radial dependence of surface coverage was observed, showing a strong peak at the axis of rotation where the influence of flow is the least. Reasonable fitting quality for our scaling theory suggests that our underlying assumptions are correct, specifically that adsorption of polyelectrolyte chains equilibrates to locally achieve $D_e \sim 1$ and that the condition is achieved with chains of increasing compactness as salt content increases. Future investigations will more rigorously test our theoretical picture by independent variation of both the spinning rate and salt concentration.

We thank the Office of Naval Research (Contract N00014-01-1-06412) and the Connnecticut Global Fuel Cell Center (Batelle Agreement #DAAB07-03-3-K-415) for financial support. A.V.D. acknowledges support of the donors of the Petroleum Research Fund, administered by the American Chemical Society under the grant PRF#39637-AC7.

APPENDIX: THEORETICAL MODEL FOR POLYELECTROLYTE ADSORPTION IN SHEAR FLOW

In this Appendix we present a Flory-like theory to describe the basic elements of layer-by-layer polyelectrolyte assembly generally in shear flow, and polyelectrolyte spin assembly (PSA) in particular. Consider adsorption of fully charged polyelectrolyte chain containing *N* Khun monomers of length *b* (for polystyrene sulfonate $b = 18$ Å) at a charged surface with surface charge number density σ (mol/m^2) from a salt solution characterized by Debye radius r_D,[24]

$$r_D = \frac{9.61}{(z^2 c)^{1/2}}\, nm \qquad \text{(A.1)}$$

for aqueous salt solutions at $T = 25$ °C with valency z and concentration c in mol/m^3. Here, we will assume that charged sites (monomers) on each polyelectrolyte chain form ionic pairs with surface charges during the adsorption process.[25] The energy of the ionic pair is equal to $-k_B T \epsilon_a$, where k_B is the Boltzmann constant, T is the absolute temperature, and ϵ_a is a dimensionless sticking energy strength. The adsorbed layer has a brush-like structure of loops [see Fig. 10(a)] with $2m$ monomers in each loop as determined by the fine interplay between the electrostatic repulsion between adsorbed chains, the elastic energy

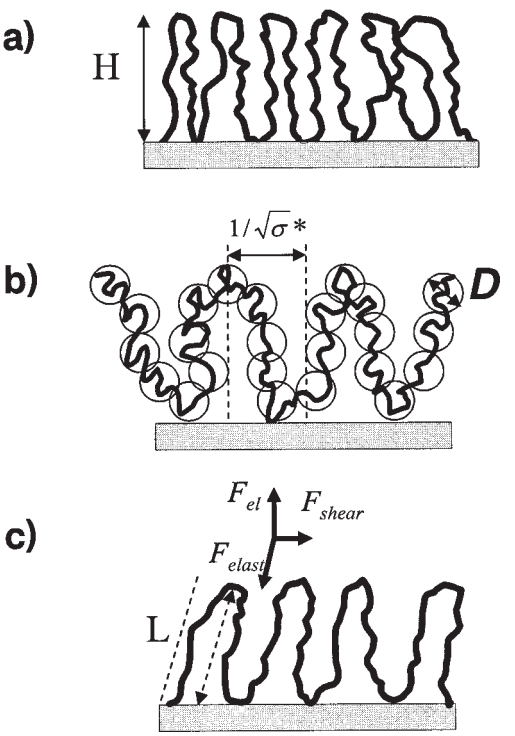

Figure 10. Schematic representation of the adsorbed layer (a) without shear; (b) without shear and with indication of Pincus blobs; and (c) under applied shear.

of each loop, and the strength of the sticking energy of ionic pair that holds the two ends of each loop attached to the surface. (1) The electrostatic repulsion energy per polymeric strand with m monomers (a half-loop) within an adsorbed layer of thickness H in the limit of high ionic strength ($H/r_D >> 1$) is estimated to be[25]:

$$\frac{F_{el}(H)}{k_B T} \approx \frac{m^2 l_B r_D^2 \sigma}{H} \tag{A.2}$$

where $l_B = e^2/\epsilon k_B T$ is the Bjerrum length that defines the length scale at which the energy of electrostatic interaction between two elementary charges e in the medium with dielectric constant ϵ is equal to the thermal energy $k_B T$. The total electrostatic energy per chain is N/m times this quantity. (2)The elastic energy per half-loop of m monomers stretched to thickness H is,

$$\frac{F_{elast}}{k_B T} \approx \frac{H^2}{m b^2} \tag{A.3}$$

Again, the total elastic energy for each adsorbed chain is (N/m) times this expression. (3) Finally, a polyelectrolyte chain with N monomers will have $N/2m$ contact points with a surface each of which contributes a favorable sticking energy $-k_B T \epsilon_a$ to the total chain-free energy. Combining electrostatic, elastic, and sticking energy terms together one obtains the following expression for the free energy of an adsorbed chain.

$$\frac{F_{ch}}{k_B T} \approx \frac{N}{m}\left(\frac{m^2 l_B r_D^2 \sigma}{H} + \frac{H^2}{m b^2} - \frac{\epsilon_a}{2}\right) \tag{A.4}$$

Minimization of the chain free energy with respect to the thickness of the adsorbed layer H gives

$$H \approx m b (u \sigma r_D^2)^{1/3} \tag{A.5}$$

where $u = l_B/b$ is the ratio of the Bjerrum length to the Kuhn length, approximately 5 for aqueous PSS. Substituting this expression into eq A.4 and simplifying we obtain the chain-free energy as function of the number of monomers m in a loop:

$$\frac{F_{ch}}{k_B T} \approx N\left((u \sigma r_D^2)^{2/3} - \frac{\epsilon_a}{2m}\right). \tag{A.6}$$

In equilibrium the chemical potential of chains in free solution is equal to that of chains in an adsorbed layer. Thus, we can set the chain free energy given by eq A.6 equal to zero. This leads to the number of monomers in each loop being:

$$m \approx \frac{\epsilon_a}{\left(u \sigma r_D^2\right)^{2/3}} \tag{A.7}$$

noting that we have dropped the factor of 2 for simplicity. The polymer surface coverage, related to the experimentally observed UV-Vis absorbance, can then be calculated using the surface charge density:

$$\Gamma \approx m\sigma \approx \frac{\sigma^{1/3} \epsilon_a}{u^{2/3} r_D^{4/3}} \tag{A.8}$$

In the case of the multilayer LbL assembly, the process reaches steady state growth with the surface charge density of the previous layer determining the thickness of the next one. The electrostatic interaction between charges in salt solutions is exponentially screened for length scales larger than r_D. We will assume that newly adsorbed chains are capable of forming ionic pairs only with the charged monomers (m for fully ionized chains) of the previous layer within thickness r_D from the top of the adsorbing layer. Thus, the effective surface charge density of each new layer, σ_{i+1}, includes only the fraction of charges presented by the adsorbed chains:

$$\sigma_{i+1} \approx \sigma_i m \frac{r_D}{H} \approx \frac{\sigma_i^{2/3} r_D^{1/3}}{u^{1/3} b} \tag{A.9}$$

For steady-state (linear) growth, each newly adsorbed layer completely reconstructs the surface properties so that $\sigma_{i+1} = \sigma_i$, leading to a surface charge density of the form:

$$\sigma^* \approx \frac{r_D}{b^2 l_B} \tag{A.10}$$

Along with eqs A.5 and A.7, this allows estimation of the adsorbed layer thickness and the number of monomers m per half-loop:

$$H \approx \epsilon_a \frac{b^2}{r_D} \quad m \approx \epsilon_a \frac{b^2}{r_D^2} \tag{A.11}$$

Both quantities increase with added salt, as $r_D \sim c^{-1/2}$; for example, the thickness of each ad-

sorbed layer increases as a square root of salt concentration, as reported experimentally by Lvov and Decher,[23] among others. For comparison with experiments, we consider the polymer surface coverage in the steady state regime, which increases with salt concentration as:

$$\Gamma \approx m\sigma^* \approx \frac{\epsilon_a}{l_B r_D}. \tag{A.12}$$

This surface coverage, measurable by UV-Vis absorption spectroscopy as the absorbance per bilayer increases as square root of salt concentration, as does the thickness, H, measurable with AFM profilometry.

To describe chain conformations inside the adsorbed layer it is useful to introduce a concept of the Pincus blob[26] of size D, which separates two different length scales. For length scales smaller than the Pincus blob size, a chain section adopts an unperturbed Gaussian conformation (at these length scales the electrostatic repulsion between neighboring chains is not strong enough to perturb chain conformations), while for length scales larger than the blob size the chains are strongly stretched by electrostatic repulsion between neighboring chains. To minimize these interactions chain sections adopt an elongated conformation of array of Pincus blobs, as shown schematically in Figure 10(b), where we have sketched a blob picture of the adsorbed layer. Each section of a chain with m monomers in this brush-like layer is stretched by the electrostatic repulsion between adsorbed chains with a force:

$$f \approx k_B T \frac{H}{mb^2} \approx k_B T \frac{r_D}{b^2} \approx \frac{k_B T}{D} \tag{A.13}$$

Inspection of this expression reveals that the Pincus blob size, $D \approx b^2/r_D$, increases as more salt is added to the solution, while the force within the loop decreases.

The development until now considered only electrostatic, elastic, and sticking energetics, with no consideration of hydrodynamic drag that may influence the adsorbed layer thickness in the present PSA process or other adsorption/flow processes. To proceed, we consider the magnitude of the shear rate that will force deformation of the Pincus blobs of size D. The shear force exerted by the external shear flow with shear rate $\dot{\gamma}$ in a solvent with viscosity η on a Pincus blob can be estimated as $F_{shear} \approx \eta\dot{\gamma}D^2$, where $D\dot{\gamma}$ is typical variance of solvent velocity on the length scale of the order of the blob size D and ηD is the blob friction coefficient within an unknown numerical prefactor. The shear flow will start deforming the Pincus blobs when the shear force, $\eta\dot{\gamma}D^2$, becomes comparable to the tension inside polymer chain, $k_B T/D$. This leads to the following condition for the crossover shear rate $\dot{\gamma}_c$.

$$\eta\dot{\gamma}_c D^2 \propto k_B T/D \tag{A.14}$$

We can rewrite this relation by introducing the relaxation time of the Pincus blob (Zimm relaxation time):[26]

$$\tau \approx \frac{\eta D^3}{k_B T} \tag{A.15a}$$

Substituting into eq A.15a an expression for the blob size $D \approx b^2/r_D$ we obtain the Zimm relaxation time

$$\tau_e \approx \frac{\eta b^3}{k_B T}\left(\frac{b}{r_D}\right)^3 \tag{A.15.b}$$

of the blob whose dimensions are controlled by electrostatic repulsion between neighboring brush strands. An external shear flow will influence the brush structure when the dimensionless group $De_e \equiv \dot{\gamma}_c\tau_e$ is of order unity.[27,28] For higher shear rates, $\dot{\gamma} > \tau_e^{-1}$, following the results of refs. 27 and 28, we assume that adsorbing chains will continue to adjust their configuration until the criterion $\dot{\gamma}\tau \approx 1$ is satisfied. For example, chains with large blob size D may feature $\dot{\gamma}\tau >> 1$ and adjust their configuration accordingly, while chains with small D will expand until $\dot{\gamma}\tau \approx 1$.

Continuing more quantitatively, we consider deformation of the adsorbed polyelectrolyte layer by shear flow with the shear rate $\dot{\gamma}$. Shear tilts the "brush" [see Fig. 10(c)] in such a way that the vector sum of (1) the shear force $F_{shear} \approx \eta\dot{\gamma}D^2$, acting at the top of the brush layer, (2) the elastic force, and (3) the electrostatic repulsive force between charged monomers $F_{el} = -\partial U_{el}(H)/\partial H$ is zero, indicating mechanical equilibrium.[27,28] The tilting of the brush results in the total brush length becoming $\sqrt{H^2+R^2}$, where R is the lateral displacement of the end point of the loops from the grafting point [see Fig. 10(b)]. The balance of projections of the forces onto normal and parallel

to the surface direction leads to two equations, respectively, dictating H, R, and m:

$$k_B T \frac{H}{mb^2} \approx k_B T \frac{m^2 l_B \sigma^* r_D^2}{H^2} \quad \text{(A.16)}$$

$$k_B T \frac{R}{mb^2} \approx \eta \dot{\gamma} D^2 \approx (\eta \dot{\gamma})^{1/3} (k_B T)^{2/3} \quad \text{(A.17)}$$

In the second equation (A.17) we use the expression for the blob size D obtained from the condition $\dot{\gamma}\tau \approx \dot{\gamma}\eta D^3/k_B T \approx 1$.[27,28] Equation A.16 yields the same relation between the height of the brush and the number of monomers in a strand m as eq A.5. Substituting the relation between H, R, and m we can write the expression of the chain free energy (single chain chemical potential) as functions of the Debye radius, shear rate, and sticking energy.

$$\frac{F_{ch}}{k_B T} \approx \frac{N}{m}\left(\frac{H^2}{mb^2} + \frac{R^2}{mb^2} - \frac{\epsilon_a}{2}\right) \approx N\left(\frac{r_D^2}{b^2} + \left(\frac{\eta \dot{\gamma} b^3}{k_B T}\right)^{2/3} - \frac{\epsilon_a}{2m}\right) \quad \text{(A.18)}$$

Setting eq A.18 to zero yields a prediction for the number of monomers per half-loop of chains adsorbing in a shear flow:

$$m \approx \frac{b^2 \epsilon_a}{r_D^2 + b^2(\dot{\gamma}\tau_0)^{2/3}} \rightarrow \frac{\epsilon_a}{(\dot{\gamma}\tau_0)^{2/3}} \quad \text{(A.19)}$$

where factoring leaves $\tau_0 \approx \eta b^3/(k_B T)$, the relaxation time of a Kuhn monomer, and the arrow indicates the limit of high shear. The crossover between electrostatic-dominated and shear-dominated regimes occurs when the Debye length r_D becomes smaller than $b(\dot{\gamma}\tau_0)^{1/3}$. Beyond this transition, the number of monomers in a brush strand decreases as the shear rate increases. Using this new expression for the number of monomers in a strand m and shear rate we can obtain the dependence of the brush thickness H and polymer surface coverage Γ:

$$H \approx bm(\sigma^* u r_D^2)^{1/3} \approx \frac{r_D \epsilon_a b^2}{r_D^2 + b^2(\dot{\gamma}\tau_0)^{2/3}} \quad \text{(A.20)}$$

$$\Gamma \approx \sigma^* m \approx \frac{\epsilon_a (r_D / l_B)}{r_D^2 + b^2(\dot{\gamma}\tau_0)^{2/3}} \quad \text{(A.21)}$$

observing that in the low-shear regime $\Gamma \propto c^{1/2}$ while in the high shear regime, $\Gamma \propto c^{-1/2}$. Due to uncertainty in absolute values for the bare relaxation time, τ_0, as well as other parameters, a more general form of eq A.21 for the purpose of data fitting is given as:

$$\Gamma \approx \alpha \frac{c^{-1/2}}{c^{-1} + \beta \dot{\gamma}^{2/3}} \quad \text{(A.22)}$$

where α and τ' are fitting parameters, c is the concentration of free ions, and $\dot{\gamma}$ is the shear rate.

Let us apply the presented above analysis to the case of polyelectrolyte spin assembly (PSA). The radial velocity profile of the liquid at point r from the center of the spinning disk rotating with angular velocity ω is:[19]

$$v(z) = \rho \omega^2 r \eta^{-1}\left(hz - \frac{z^2}{2}\right) \quad \text{(A.23)}$$

where h is film thickness, and ρ is the density of a liquid. Close to the surface of a disk this velocity profile can be approximated by the first term. In this case, the shear rate is equal to

$$\dot{\gamma} = \rho \omega^2 r h / \eta \quad \text{(A.24)}$$

The shear rate increases linearly with distance r from the center of a disk. In this case, close to the center of a disk the shear rate is not strong enough to perturb adsorbed layer, and the thickness of the adsorbed layer and polymer surface coverage are given by eqs. A.11 and A.12. Substituting A.24 into A.21 reveals that the flow may significantly influence the layer structure for distances r larger than

$$r_{flow} \approx \frac{\eta}{\tau_0 \rho \omega^2 h}\left(\frac{r_D}{b}\right)^3 \quad \text{(A.25)}$$

beyond which the flow term of eq A.21 becomes dominant. For distances $r >> r_{flow}$ the polymer surface coverage decays with distance r as $\Gamma \sim r^{-2/3}$, while for radii in the transition region (the case in our experiments) a more complete expression is required to described the observed data, namely:

$$\Gamma \approx \frac{\Gamma_0}{1 + \zeta \cdot (\omega^2 r)^{2/3}} \quad \text{(A.26)}$$

where Γ_0 and ζ are fitting parameters.

The above development allows fitting of experimental data and subsequent estimation of behavior beyond that observed, with the quality of fitting allows us to gauge the applicability of concepts incorporated into the theory and acceptability of mathematical simplifications.

REFERENCES AND NOTES

1. Iler, R. K. J Colloid Interface Sci 1966, 21, 569.
2. Decher, G.; Hong, J. D. Ber Bunsen-Ges Phys Chem 1991, 95, 1430.
3. Decher, G.; Hong, J. D. Makromol Chem, Macromol Symp 1991, 46, 321.
4. Decher, G. In The Polymeric Materials Encyclopedia: Synthesis, Properties and Applications; CRC Press, Boca Raton, FL, 1996.
5. Decher, G. Science 1997, 277, 1232.
6. Hammond, P. T. Curr Opin Colloid Interface Sci 1999, 6, 430.
7. Decher, G.; Eckle, M.; Schmitt, J.; Struth, B. Curr Opin Colloid Interface Sci 1998, 3, 32.
8. Schoeler, B.; Kumaraswamy, G.; Caruso, F. Macromolecules 2002, 35, 889.
9. Kim, D. K.; Han, S. W.; Kim, C. H.; Hong, J. D.; Kim, K. Thin Solid Films 1999, 350, 153.
10. Schmitt, J.; Grunewald, T.; Decher, G.; Pershan, P. S.; Kjaer, K.; Losche, M. Macromolecules 1993, 26, 7058.
11. Cho, J.; Char, K.; Hong, J.-D. Adv Mater 2001, 13, 1076.
12. Chiarelli, P. A.; Johal, M. S.; Casson, J. L.; Roberts, J. B.; Robinson, J. M.; Wang, H.-L. Adv Mater 2001, 13, 1167.
13. Lee, S.-S.; Hong, J.-D.; Kim, C. H.; Kim, K.; Koo, J. P.; Lee, K.-B. Macromolecules 2001, 34, 5358.
14. Joly, S.; Kane, R.; Radzilowski, L.; Wang, T.; Wu, A.; Cohen, R. E.; Thomas, E. L.; Rubner, M. F. Langmuir 2000, 16, 1354.
15. Shiratori, S. S.; Rubner, M. F. Macromolecules 2000, 33, 4213.
16. Ferreira, M.; Rubner, M. F. Macromolecules 1995, 28, 7107.
17. McAloney, R. A.; Sinyor, M.; Dudnik, V.; Goh, M. C. Langmuir 2001, 17, 6655.
18. Johal, M. S.; Casson, J. L.; Chiarelli, P. A.; Liu, D.-G.; Shaw, J. A.; Robinson, J. M.; Wang, H.-L. Langmuir 2003, 19, 8876.
19. Emslie, A. G.; Bonner, F. T.; Peck, L. G. J Appl Phys 1958, 29, 858.
20. Meyerhofer, D. J Appl Phys 1978, 49, 3993.
21. Schlenoff, J. B.; Ly, H.; Li, M. J Am Chem Soc 1998, 120, 7626.
22. Dubas, S. T.; Schlenoff, J. B. Macromolecules 1999, 32, 8153.
23. Lvov, Y. M.; Decher, G. Crystallogr Rep 1994, 39, 628.
24. Probstein, R. F. Physicochemical Hydrodynamics, An Introduction; John Wiley &Sons, Inc.: New York, 1994.
25. Park, S. Y.; Rubner, M. F.; Mayes, A. M. Langmuir 2002, 18, 9600.
26. Rubinstein, M.; Colby, R. H. Polymer Physics; Oxford University Press, New York, 2003.
27. Harden, J. L.; Cates, M. E. Phys Rev E 1996, 53, 3782.
28. Rabin, Y.; Alexander, S. Europhys Lett 1990, 13, 49.